RESEARCH OF INTEREST TO THE NASA RESEARCH AND TECHNOLOGY ADVISORY COMMITTEE ON MATERIALS AND STRUCTURES

December 14-15, 1976

NASA-Ames Research Center
Moffett Field, California

TABLE OF CONTENTS

TABLE OF CONTENTS

(Continued)

Aerodynamic Research Branch

1. Advanced Subsonic and Supersonic Paneling Method
2. Two-Dimensional Transonic Unsteady Aerodynamics
3. Aero-Optical Interactions
4. Aircraft Buffet

ADVANCED SUBSONIC AND SUPERSONIC PANELING METHOD. An advanced aerodynamic surface paneling method is being developed by the Boeing Commercial Airplane Company under contract to Ames Research Center. The method is applicable to both subsonic and supersonic flow, as represented by linearized potential flow theory. The method is based on linearly varying sources and quadratically varying doublets which are distributed over flat or curved panels. Numerical results produced to date have illustrated the following features:

1. The paneling can be applied to the true surface geometry of arbitrarily shaped aerodynamic configurations. Thus, the analyst does not have to make approximations to the true geometry.

2. Both subsonic and supersonic analysis, and subsonic design problems can be solved. In the design mode, the geometry required to produce a specified pressure distribution is determined. One or more components of a configuration can be designed in the presence of other components whose geometrical shapes are fixed.

3. The method offers the user a variety of modeling options. For example, for wing-like components all the usual thin surface approximations are available; for more accurate results the paneling and boundary conditions can be applied to the wing upper and lower surfaces. For closed bodies, either velocity of potential type boundary conditions can be imposed.

4. The method is both stable and accurate. Unlike other methods, the numerical results display a marked insensitivity to the size, shape, and arrangement of panels. Thus, the paneling can be based on the geometry and physics of the configuration (e.g., higher density paneling in regions of large pressure gradients) rather than on paneling rules which must be followed to avoid spurious numerical results. This insensitivity to paneling layout also makes automated paneling a practical possibility. Good accuracy is obtained with relatively sparse panel densities; convergence to highly accurate results occurs at moderate panel densities.

5. The method is efficient. Individual panel AIC calculation times are competitive with existing body surface paneling methods and overall matrix sizes are

much smaller because of the reduced number of panels required. In addition, the AIC integrals are all evaluated in closed form, thus avoiding the problems associated with numerical integration of singular integrals.

The method is also being extended to unsteady flow.

References:

1. Johnson, F. T., and Rubbert, P. E.: Advanced Panel-Type Influence Coefficient Methods Applied to Subsonic Flows. AIAA Paper 75-50, January 1975.

2. Ehlers, F. E., Johnson, F. T., and Rubbert, P. E.: A Higher Order Panel Method for Linearized Supersonic Flow. AIAA Paper 76-381, July 1976.

(L. Erickson)

TWO-DIMENSIONAL TRANSONIC UNSTEADY AERODYNAMICS. A description of the Ames Aerodynamics Division program on unsteady aerodynamics was presented in the previous RTAC report from Ames. Since the last submission, significant progress has been made and schedules have been set for the installation of the 2-D oscillating airfoil apparatus in the Ames 11- by 11-foot Transonic Wind Tunnel and the first tests. The design of the apparatus and models is complete. Initial laboratory tests of the oscillating rig will commence in January 1977. The wing models will be constructed of graphite-epoxy composite materials and will be completed by March 1977. The first three airfoil sections to be fabricated will be a NACA 64A010, a supercritical airfoil section, and an advanced helicopter rotor section. The tests in the 11- by 11-foot Transonic Tunnel are scheduled for July 1977.

A non-oscillatory model of the proposed apparatus was constructed and tested in the Ames 2- by 2-foot Transonic Wind Tunnel during April and May of 1976. The results of this test, which were reported at a recent meeting of the Supersonic Tunnel Association, showed that a high-quality two-dimensional flow can be realized in the 2-D channel formed by the splitter plates which support the airfoil model.

The mini-computer based data acquisition and control system will be first used in a small-scale test in a low speed 25- by 35 cm vacuum wind tunnel. The purpose of this test, aside from its use as a software verification tool, is to assess the validity of the Kutta condition in an unsteady flow. Unsteady pressure measurements will be made in the vicinity of the trailing edge of a NACA 64A010 airfoil pitching about a fixed axis near the 25% chord. The unsteady loading will be compared to theory and the frequency above which the Kutta condition fails will be measured.

(S. S. Davis)

AERO-OPTICAL INTERACTIONS. In a cooperative effort between NASA-Ames and the Air Force Weapons Lab, transonic wind tunnel tests have recently been made to obtain the optical and aerodynamic properties of a flow over a cavity, with and without various devices for inhibiting resonance. As reported previously to the committee, the tests were for the purpose of evaluating and minimizing the density disturbances which degrade electromagnetic waves propagating into or out of the cavity. The tests included measurements of modulation transfer function, line-spread function, holograms, hot-wire currents, particle velocities from laser-doppler interferograms, pressure fluctuations, and force fluctuations on a ball probe. Devices for inhibiting resonance included porous cavity walls, porous spoilers ahead of the cavity, and air injected through the forward cavity wall. A repeat of previous flat-plate tests was also made for comparison.

Preliminary data analyses indicate that the devices which are effective in inhibiting cavity resonance were generally detrimental to wave propagation and that satisfactory performance will have to be effected by compromise between the loads and propagation requirements. Some success was achieved in computing optical degradation from the aerodynamic measurements. Data analysis is proceeding to further examine the relationship between the various measurements.

Preparations are about complete for wind tunnel tests of the turret-fairing combination to be mounted on the Air Force Airborne Laser Laboratory.

(D. A. Buell)

AIRCRAFT BUFFET. The research at Ames on aircraft buffet, as previously reported to this Committee, is continuing toward its objectives to define the unsteady aerodynamic inputs and structural response characteristics of wind-tunnel models and flight vehicles and to investigate methods of aircraft buffet intensity prediction. Configurations investigated include the F-111A, F-111/TACT, and F-5A. A contract is in progress with General Dynamics Corporation to compare flight buffet characteristics of the F-111A with predictions based on wind tunnel unsteady pressure measurements obtained by Ames from 1/6-scale semispan model. A contract is also in progress with Northrop Corporation to make similar comparisons between wind tunnel and flight data on the F-5A. The Northrop contract also includes the study of the wing rock problem and associated unsteady aerodynamic loads. The TACT buffet investigation is being conducted jointly by Ames, AFFDL and DFRC.

Since the last report to the Committee, the wind tunnel tests of 1/6-scale aluminum and steel models of the F-111/TACT have been completed which will provide information on the effects of flexibility on the fluctuating pressures that cause buffet. Tests were also completed by Northrop at Ames of a full-span model of the F-5A mounted on an apparatus that allowed a controlled freedom in roll motion. Each of these models had extensive unsteady pressure instrumentation. Analysis of the data from all these tests is now in progress.

(C. F. Coe)

Chemical Research Projects Office

1. Fire Safe Materials for Aircraft Interiors
2. Laser Resistant Materials Effects Program
3. Elastomers for Aircraft Tires
4. Supersonic Aircraft Fuel Tank Sealants

FIRE SAFE MATERIALS FOR AIRCRAFT INTERIORS. The thermochemical and flammability characteristics of some typical thermoplastic materials currently in use and others being considered for use in aircraft interiors were determined. The properties studied included; (1) thermomechanical properties such as glass transition and melt temperature, (2) changes in polymer enthalpy by differential scanning calorimetry, (3) thermogravimetric analysis in anaerobic and oxidative environments, (4) oxygen index, (5) smoke evolution, (6) relative toxicity of the volatile products of pyrolysis, and (7) selected physical properties. The generic polymers that were evaluated included; acrylonitrile butadiene styrene, bisphenol A polycarbonate, 9,9 bis (4-hydroxyphenyl) fluorene polycarbonate-poly (dimethylsiloxane) block polymer, phenolphthalein-bisphenol A polycarbonate, phenolphthalein polycarbonate, polyether sulfone, polyphenylene oxide, polyphenylene sulfide, polyaryl sulfone, chlorinated polyvinyl chloride homopolymer, polyvinyl fluoride, and polyvinylidene fluoride. Processing parameters, including molding characteristics of some of the advanced polymers, are described. Tests results and relative rankings of some of the flammability, smoke, and toxicity properties were determined. Under these test conditions some of the advanced polymers evaluated were significantly less flammable and toxic or equivalent to polymers in current use.

(D. Kourtides)

LASER RESISTANT MATERIALS EFFECTS PROGRAM. Chemical and thermal phenomena are not exclusive mechanisms of ablation occurring in polymer laser protection systems. Char layers formed during exposure are subject to external as well as internal stresses which can cause mechanical thermal spallation.

A study is underway to assess the extent of mechanical thermal spallation for an EX112 canopy polymer system. Experimental data from a series of laser tests is being analyzed to interpret the discontinuity in material performance in terms of mechanical thermal spallation. The present modified CMA model used to predict performance of the EX112 material without spallation will be upgraded to incorporate spallation, if possible, to obtain better agreement between experiment and prediction. This data then will be used in an attempt to synthesize polymers with improved performance based on critical physical parameters.

The CO_2 laser effects on low density PBI composites has been performed by Wright-Patterson Air Force Base (AFML), and the test results and ablation rates are given in Table 1. The data comparison to the EX-112 material was used only for point of interest and not for specific comparisons.

(D. E. Cagliostro and S. R. Riccitiello)

SAMPLE TYPE	SAMPLE #	ENERGY DENSITY cm^2	TIME sec	SPOT SIZE (cm^2)	Kj	DEPTH (a) OF CHAR	TOTAL (b) THICK	Kj/cm^2	(a/b) Kj/cm^2	AIR NO AIR
PBI FOAM	1 (a) 1 (b)	0	1.0	.33	0.858	0.60 0.62	2.312 2.295	.236 .238	.102 .104	NO AIR NO AIR
PBI FOAM	2	2.60	1.0	.33	0.858	0.560	2.109	[illegible]	.102	NO AIR
PBI FOAM	3	2.39	1.07	4.52*	10.8	1.173	1.951	.49	.252	NO AIR
PBI FOAM	4	2.15	1.09	4.52*	11.07	1.872	1.372	.76	.408	NO AIR
PBI FOAM	5	2.60	1.0	.33	0.858	0.710	2.075	.272	.131	NO AIR
EX 112	1	2.60	1.0	.33	0.858	0.021	0.408	.008	.0198	NO AIR
EX 112	2	[illegible]	5.0	.33	[illegible]29	0.054	0.[illegible]3	.004	.0102	NO AIR

*SAMPLE IRRADIATED BY EAL LASER

a SAME AS VIRGIN MATERIAL RECESSION

$\therefore \frac{a}{Kj/cm^2}$ IS RATE OF RECESSION

$\frac{a}{b}$ IS ACTUAL PERCENT OF MATERIAL LOST BASED ON STARTING THICKNESS

$\therefore$ a/b/Kj/cm^2 IS RATE PERCENT OF VIRGIN MATERIAL RECESSION

Table 1.

ELASTOMERS FOR AIRCRAFT TIRES. The goal of improved aircraft tire treads continues to be pursued by fundamental and developmental work on various tire elastomers: natural rubber (NR) or cis-1,4-polyisoprene, cis-1, 4-polybutadiene (CB), vinyl or 1,2-polybutadiene (VB), and trans-polypentenamer (TP). Along fundamental lines, a comparative investigation of the oxidation of these elastomers has resulted in the preparation and/or presentation, at chemistry conferences, of papers on the thermal and photosensitized oxidation of NR and CB, with corresponding work being underway on VB and TP. Related fundamental work involves a study of the abrasion mechanisms for tread elastomers and proposed new elastomer-elastomer adhesion studies. Along developmental lines, a set of 75/25 NR/VB-retreaded tires were flight-tested on an FAA B-727 aircraft and found to exhibit improved wear over that of the 75/25 NR/CB control tires. A paper describing those tires was presented at the Aircraft Safety and Operating Problems Conference, Langley, October 1976. As a follow-up to that work, a new set of 50 NR/VB tires will be fabricated to obtain statistical wear data in actual airline service. In a parallel effort on NR/TP-retreaded tires, a tire has been fabricated for dynamometer certification; once this is accomplished, a full set of NR/TP tires will be fabricated to obtain statistical wear data in actual airline service. In a parallel effort on NR/TP-retreaded tires, a tire has been fabricated for dynamometer certification; once this is accomplished, a full set of NR/TP tires will be fabricated for evaluation in Langley tract tests and in FAA flight tests. Further developmental work involves Langley small aircraft tire tests being carried out on sixty 22x5.5 tires having NR, NR/CB, or NR/TP treads. Several tires of each tread type have been instrumented for dynamic studies under various operational modes.

(M. A. Golub and S. R. Riccitiello)

SUPERSONIC AIRCRAFT FUEL TANK SEALANTS. Advanced Supersonic Aircraft Fuel Tank Sealants - Test specimens of various fluorosilicone sealants installed in the YF-21A aircraft fuel tanks in 1975 are currently being flight tested. More than 36 flights of 2-3 hours duration each have been made. Inspection of the fuel tank sealand test specimens was made in June 1976 and very little change was noted. A decision was made to continue the adhesion, weight and volume loss tests until January 1977 at which time inspection will be made again.

The optimization and characterization of new Ames sealant elastomer candidates is proceeding. These materials, a fluoroether triazine and a fluoroether-1,2,4-oxadiazole, are being cross-linked and studied for eventual selection. These represent essential steps in ultimately achieving the appropriate physical properties suitable for a supersonic fuel tank sealant application.

(R. Rosser)

Materials & Physical Sciences Branch

1. Band Structure Calculation of Crystalline Solids by the Empirical Pseudopotential Method

2. Theoretical Studies of the Adsorption of Co on Copper Surfaces

3. Relativistic Fffects in Small Catalytic Clusters

4. Radiation Blockage Calculations for Candidate Heat Shield Materials for Jupiter Entry

5. Relativistic Wavefunctions and Properties for Atoms with Atomic Numbers 2 through 106

6. A New Experimental System for the Study of Low Pressure Chemical Reactions on Particulate Metal Catalysts

7. Environmental Effects on the Fatigue Properties of Graphite-Epoxy

8. Fatigue Damage Accumulation in Graphite/Epoxy Composite Laminates

9. The Preparation of Model Catalytic Particles Supported on Alumina

10. Coadsorption of Cesium on Oxygen on W(100)

11. Present Status of the Auger-Microprobe Development

Materials & Physical Sciences Branch

12. Co-Adsorption of Cu and C on (100)W

13. Oxide Formation on Single Crystalline Copper-Nickel Alloy Thin Films

14. Corrosion of Structural Engineering Materials in Coal Gasification Environments

15. The Kinetics of Hydrogen Chemisorption Onto Evaporated Iron Films

16. The Kinetics of the Incubation Period of Hydrogen Attack in Low Carbon Steels

17. Stress Corrosion of Zircaloy

18. Hydrogen-Enhanced Crack Growth in a Low Strength Ferritic Steel

19. The Kinetics of Oxygen (O) and Hydrogen Sulfide (H_2S) Chemisorption Onto Evaporated Iron (Fe) Films

20. The Surface Mobility of Small Metal Clusters

21. The Adsorption and Early Stages of Ag and Au on W Single Crystal Surfaces

BAND STRUCTURE CALCULATION OF CRYSTALLINE SOLIDS BY THE EMPIRICAL PSEUDOPOTENTIAL METHOD. Band structure calculation of all group V and group VI transition metals (Nb, V, Ta, W, Mo) of BCC structure have been completed. From these band structure calculations other physical properties such as transition reflectivity, density of states and Fermi surfaces have been calculated. These results have been compared with the available experimental results. The agreement between the calculated properties and the experimental results are very good. Presently, the work is focused on calculating the charge distribution of these crystals. In the future this work will lead to calculations of electron-phonon coupling and will aid in the search for higher superconducting transition temperature material.

(C. G. Sridhar, C. Y. Fong and E. E. Whiting)

THEORETICAL STUDIES OF THE ADSORPTION OF CO ON COPPER SURFACES. Two geometries of CO chemisorbed on a Cu(100) surface have been studied using the self-consistent field $X\alpha$ scattered-wave method. Both geometries assume the CO molecule is bonded to the Cu surface with the C end down; one geometry is in the four-fold symmetric hole site and one is directly on top of a copper atom. In the hole site, CO and the five nearest-neighbor Cu atoms are included in the calculation. In the direct adsorption case, CO and the Cu atom directly below are included in the calculation.

The calculated ground state (G.S.) and transition state (T.S.) of the $CO(Cu)_5$ cluster are shown in Figure 1. After using a Guassian broadening function on the T.S. energies, the valence density of states (DOS) is obtained. This DOS for the four-fold symmetry case gives a satisfactory interpretation of the two main peaks (α and β) and the copper d band in the UV photo emission spectrum (UPS, Ref. 1). A third weaker peak (γ) of the UPS data can be correlated with a CO molecule adsorbed directly on top of a copper atom. All these peaks in the UPS spectrum can be accounted for by considering the CO adsorbed onto the Cu surface in these two different geometries. On the basis of our calculations, we believe that both types of CO chemisorption occur simultaneously even at low coverages. Similar calculations are underway for O and W and H on Ni.

Reference:

1. Demuth, J. E. and Eastman, D. E. (to be published in Solid State Comm.)

(H. L. Yu)

COMPARISON BETWEEN THE DENSITY OF STATES OF THE $CO(Cu)_5$ CLUSTER AND THE UV PHOTOEMISSION SPECTRUM

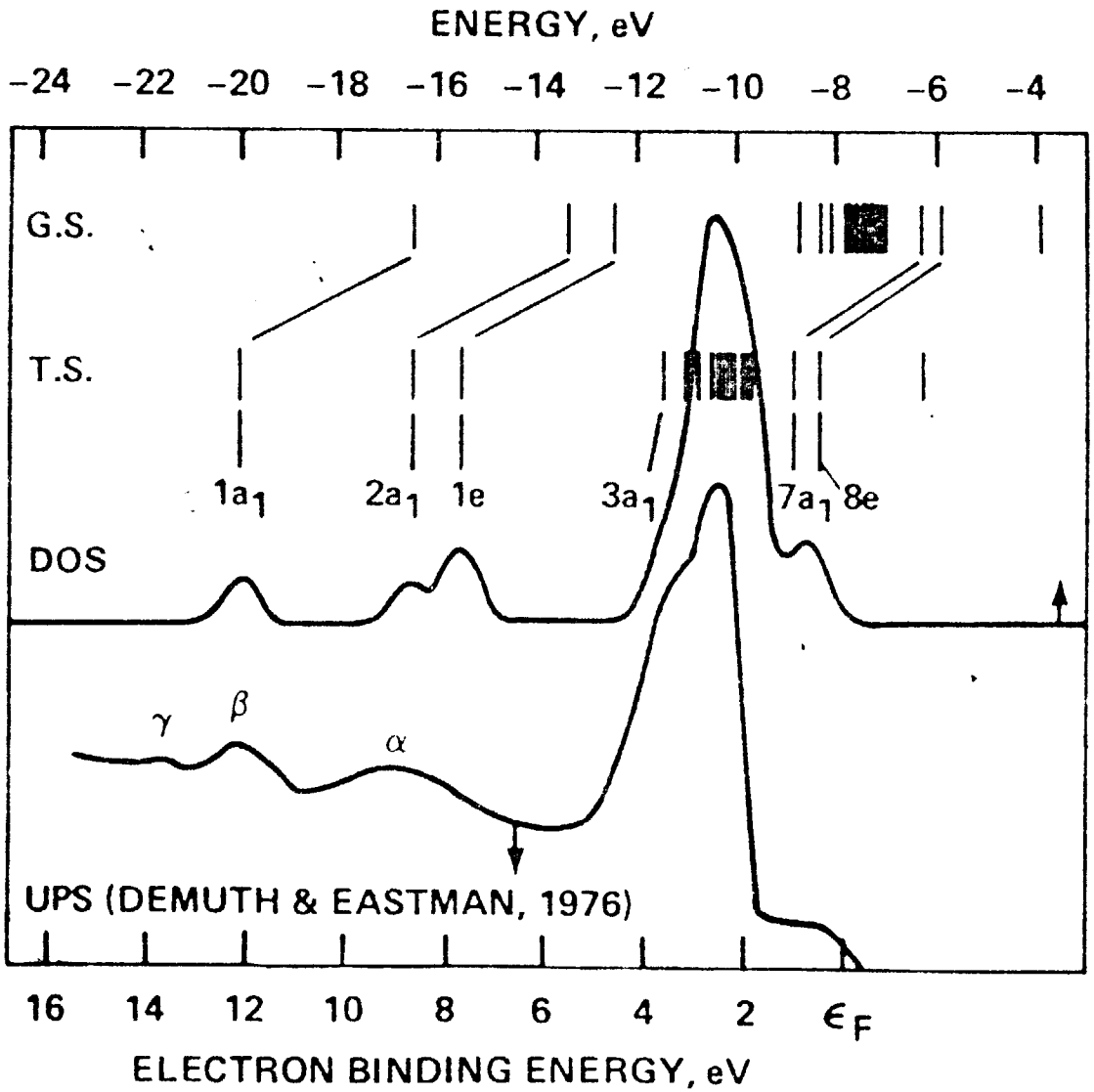

RELATIVISTIC EFFECTS IN SMALL CATALYTIC CLUSTERS. Electronic structure calculations have been performed on tetrahedral clusters of Pt and Pd using the relativistic version of the X_α-scattered-wave method. Results for Pt led to the expectation that relativistic effects could play an important role in the interaction of a heavy metal with an adsorbate. Further calculations were then carried out with the clusters HPt_4 and HPd_4 where H sits at the center of the tetrahedron. This cluster represents a simplified model for both the adsorption and absorption of hydrogen by transition metal aggregates. It is concluded from these calculations that relativistic effects have to be considered in order to account for the significantly higher H-solubility in Pd.

(C. Y. Yang)

RADIATION BLOCKAGE CALCULATIONS FOR CANDIDATE HEAT SHIELD MATERIALS FOR JUPITER ENTRY. Studies have been initiated to calculate the molecular constants necessary to improve estimates of the amount of radiative energy blocked, i.e., absorbed, by ablation products which will form on heat shields made from three candidate materials at Jupiter entry conditions. Work on the volume reflecting material (SiO_2) has demonstrated that a band system of SiO, $X^1\Sigma^+ \rightarrow E^1\Sigma^+$, will heavily absorb the brilliant intensity from three atomic silicon lines originating in the mixing region between the boundary layer and the high-temperature inviscid portion of the shock layer. The blockage of these lines is quite significant because they lie in the spectral region between 1700 and 2300 Å and emission in this region would be absorbed in the heat shield if it were not absorbed in the boundary layer. The demonstration was accomplished in two parts: (1) Wavefunctions and electronic transition moment calculations were performed and the transition moment results agree well with the single set of data available from experiment; and (2) a one-dimensional radiative transport calculation was performed which used the theoretical electronic transition moment as input and which correctly modeled the rotational structure of the transition of SiO specified above. These calculations demonstrated that the emission from inviscid and mixing regions of the shock layer in the wavelength range between 1700 - 2300 Å is reduced

by 1-2 orders of magnitude when the SiO $X^1\Sigma^+$-$E^1\Sigma^+$ transition is accounted for. Similar calculations on the $X^1\Sigma^+$ - $A^1\Pi$ transition are nearly complete, and work is proceeding on the species C_3, C_2 and CO of interest for the carbon and carbon phenolic heat shields.

(S. R. Langhoff and J. O. Arnold)

RELATIVISTIC WAVEFUNCTIONS AND PROPERTIES FOR ATOMS WITH ATOMIC NUMBERS 2 THROUGH 106. A complete set of relaxed-orbital electron binding energies and other selected properties have been calculated relativistically for atoms from helium through element 106. The following quantities have been tabulated: binding energies, total energies, electron kinetic energies, electron-nucleus potential energies consisting of electrostatic and Breit interaction terms, vacuum polarization energies, and 1s self energies. A separate listing of Slater integrals has been compiled. These results will form the basis for computations of inner-shell transition rates and relativistic fluorescence yields and are likely to be applied extensively in the interpretation of Auger and X-ray photo-electron spectrometric data.

In addition to the four compendia of atomic properties mentioned above, twelve journal articles have resulted from this research.

(B. Craseman, Univ. of Oregon and H. Mark)

A NEW EXPERIMENTAL SYSTEM FOR THE STUDY OF LOW PRESSURE CHEMICAL REACTIONS ON PARTICULATE METAL CATALYSTS. Previous experimental attempts to investigate the catalytic properties of particulate metal catalysts on supportive substrates, with various reactive gases as a function of the size, morphology, and orientation of the particles have not been satisfactorily performed. This is because previous investigations have been unable to:

1. Produce particles of metal catalysts that are well controlled in terms of size, morphology, and orientation.

2. Conduct the experiments in an environment of cleanliness that would tend to eliminate the possibility of impurities influencing the results.

3. Evaluate the changes in the physical characteristics of the metal particles after exposure to chemical and thermal conditions that are typical of a catalytic environment.

The objective of this experimental program is to perform the first definitive UHV investigation of the role the physical properties of particulate metal catalysts (i.e., size, orientation, morphology, etc.) may play in determining the catalytic activity of the material. In order to do this, a special UHV system has been assembled which is shown schematically in Fig. 1. The system consists of two chambers which can be partially isolated from one another and separately operated at pressures of approximately 10^{-9} torr. The preparation chamber is used to generate a particulate metal catalyst by e-beam evaporation of an active metal onto a clean, in-situ cleaved substrate of (001) mica. Catalytic materials such as Ni, Pd and Pt on mica will be used in this study.

The deposition oven in the first chamber is used to control the mica substrate temperature and a quartz crystal microbalance is used to monitor the impingement flux of the active metal during deposition. By controlling the substrate temperature, flux, and deposition time, it is possible to generate a variety of particles having various sizes, densities, morphologies, and orientations. These properties can be determined by such methods as transmission electron microscopy (TEM), transmission electron diffraction (TED), and statistical size analysis. As an example, Fig. 2 shows a series of pictures of Pd on mica and demonstrates some of the physical variations that can be produced in the particles by varying the deposition parameters. In this case the Pd particle sizes and densities were varied by fixing the impingement flux and deposition time and varying the substrate temperature.

From a correlation of desorption data and particle structure etc., it should be possible to evaluate the role that the physical properties of the particles play in determining the catalytic potential of a particulate, supported metal catalyst. In fact, with the techniques available (TEM/TED) the effects of thermal and/or chemical exposure on the physical properties of individual crystallites should be easily determined and it is hoped that a statistical correlation may be established between observed changes in individual crystallites and gross changes in the chemical activity of the catalytic materials studied in this work.

(M. Thomas, R. D. Moorhead and H. Poppa)

ENVIRONMENTAL EFFECTS ON THE FATIGUE PROPERTIES OF GRAPHITE-EPOXY. The effects of air and water environments on the torsional and flexural fatigue properties of advanced graphite-epoxy structural composites were investigated at 24°C and 74°C. Tests were run using electro-hydraulic test systems at stress ratios of R = 0 (zero to maximum, repeated) and R = -1 (zero mean stress). Materials investigated were AS/3501 and T300/934, with fiber orentiations of unidirectional $[0°]_{16}$, angleply $[0/\pm45/0°]_{2s}$, $[0/\pm30/0°]_{2s}$, and woven fiber cloth. Results indicate that both a water environment and a higher test temperature contribute to degradation of stiffness in all materials during both torsion and flexural cycling. Damage is much greater with R = -1 compared with R = 0 cycling. The effect of environment is also greater in the fully reversed cycling tests. The accumulation of fatigue damage (reduction in stiffness) in water at room temperature and in air at 74°C is similar but slightly greater than that in ambient air at room temperature. However, the combination of increased temperature (74°C) and water produced significantly greater degradation of stiffness under both torsional and flexural cyclic stress than in room temperature air. Flexure fatigue results showed a large fatigue effect, with $[0/\pm30/0°]_{2s}$, for example, showing fatigue limits of less than 50% and 30% of the static failure strength for specimens tested under stress ratios of R = 0 and R - 1, respectively. Compliance measurements indicated that the final failures are preceded by damage initiation and accumulation, which begins at about 1% of the specimen's fatigue life.

(H. T. Sumsion)

FATIGUE DAMAGE ACCUMULATION IN GRAPHITE/EPOXY COMPOSITE LAMINATES. The accumulation of fatigue damage in notched graphite/epoxy composite laminates (AS/3501 and T300/934) under tension-tension (T-T) and tension-compression (T-C) loading has been investigated. In T-T cycling (R=0, σ_{max} = 85% notched strength) fatigue damage in the $[0|\pm\theta|0]_s$ and $[0|\pm\theta|0]_s$ laminates (θ=30° or 45°) occurred mainly in the form of splits at notch roots and hole edges, which intensified and propagated vertically with increasing numbers of cycles. As a consequence of this notch root blunting effect, the residual strength (σ_γ) increased by about 40% at 2 x 10^6 cycles, while the corresponding increase in compliance was about 5%. Fatigue damage at 2 x 10^6 cycles was confined to the region between splits at hole edges or between specimen edge and notch root split for edge-notches.

Transverse spread of damage from holes and notch roots was very slight, if any. No fatigue failure was possible at this stress level which corresponded to about 50% of unnotched strength. At higher cyclic stress ranges ($\Delta\sigma$), (imposed on pre-cycled specimens), σ_γ increased to unnotched level for holes and to about 80% of the unnotched strength for sharp notches. In either case, fatigue failure occurred at a $\Delta\sigma$ equal to about 70% of unnotched strength through general unnotched fatigue mechanisms operating in the net section. The results demonstrate the insensitivity of these laminates to T-T fatigue in the notched condition. The $[0|\pm45|90]_s$ laminate, in contrast, is susceptible to T-T fatigue failures at stress levels of the order of 50% of its unnotched strength, both in the notched and unnotched condition. σ_γ increases by about 15% at 10^6 cycles when cycled at a $\Delta\sigma$ equal to 85% notched strength (60% unnotched strength) but thereafter decreases sharply, resulting in fatigue failure at 2×10^6 cycles. Concomitant increase in specimen compliance is about 20% at 10^6 cycles. Fatigue damage is initially contained between splits at hole edges, except for progressive failure of 90° plies across the specimen width. However, the onset of edge delamination beyond 10^5 cycles at this stress level and its gradual progress across the specimen width is identified as the principal cause of fatigue failure of this laminate. The role of notch in effecting fatigue failure is at most of a secondary nature. Under T-C cycling conditions, for all laminates, fatigue damage was observed to propagate from the edge notches into the interior of the specimen and failure occurred when a critical amount of damage had built-up ahead of a notch root. The rate of accumulation of fatigue damage under T-C loading could be described by two distinct stages. The first stage, characterized by a linear crack-opening displacement range versus cycles relation (ΔCOD-N) and relatively low damage growth rates occupied the major proportion of specimen life. The second stage, in which ΔCOD increased exponentially with N represented the terminal events leading to specimen failure. A critical ΔCOD existed for failure. The concept established demonstrates that resistance to damage accumulation in T-C fatigue can be effectively compared for various laminates by measuring changes in ΔCOD during cycling.

(S. V. Ramani)

THE PREPARATION OF MODEL CATALYTIC PARTICLES SUPPORTED ON ALUMINA. It is known that the catalytic activity and the selectivity of certain chemical reactions depend upon particle size distribution, particle density and orientation of the supported metal crystallites. At present, most dispersion relations describing average particle sizes are derived indirectly from BET adsorption isotherms, and only a few orientational relationships to respective substrates have been reported in the literature. However, direct observation can be employed to determine the exact crystallographic nature of the supported metal catalysts. The main difficulty is that very special experimental particle analysis techniques are required and that practical thin support materials (i.e., alumina) have to be prepared.

Using thin amorphous alumina as a starting material, various phases of thin alumina film have now been prepared by phase transformation during heating.[1] The metal vapor deposit/substrate interaction is then studied on these substrates by using in-situ TEM (transmission electron microscopy) which is particularly suitable for this kind of research.

The results show that the deposit growth characteristics such as particle density, size distribution, morphology, and orientation are strongly dependent upon the substrate phase, orientation and upon the deposition conditions. The information obtained in this investigation will be used to generate desired catalytic particles, and the kinetics of chemical reactions on various types of catalytic crystallites will be studied in future investigations.

Reference:

1. Eal H. Lee and Helmut Poppa; J. Vac. Sci. Tech., Jan/Feb, Special Proceedings (1976).

(E. H. Lee and H. Poppa)

COADSORPTION OF CESIUM AND OXYGEN ON W(110). This research is motivated by the need to reduce the collector work-function in thermionic converters to around 1 eV, so as to increase the converter efficiency to over 20%. A previous study (Ref. 1) showed that such low work-function values could be obtained on W(100) either by submonolayer coadsorption of cesium and oxygen, or by multilayer growth of cesium oxide. So W(110) has been chosen for the present study to examine in particular, the influence of the substrate surface crystallographic properties on the adsorption and condensation of Cs and oxygen on W.

A sketch of the surface analytical apparatus is given in Fig. 1. Various techniques are combined in the UHV chamber: relative coverages are determined, and the cleanliness is checked by Auger electron spectroscopy (AES; adsorbate order and respective structures are studied by low energy electron diffraction (LEED); work-function change is monitored by an electron beam retarding field method; thermal desorption spectroscopy is performed by heating the sample in front of a quadrupole mass spectrometer, or for cesium alone with a surface ionization detector. Cesium is provided either by a zeolite ion gun or, in a much cleaner way, by a Knudsen effusion cell. Oxygen gas can be leaked into the chamber. The W(110) sample temperature can be varied between 250°K and 2500°K.

A brief study of oxygen adsorption on W(110) at room temperature provided results in essential agreement with the latest and most extensive study of that system to date (Ref. 2).

Cesium adsorption was examined more thoroughly, because very few results are available on the Cs/W(110) ionic adsorption system. The validity of work-function and coverage values, obtained previously (Ref. 3) without a direct proof of the surface cleanliness, was confirmed.

It was shown then that the desorption conditions need to be specified, when determining neutral desorption energies, as cesium can also be desorbed in the ionic state Cs^+. As shown in Fig. 2, preventing ionic desorption broadens and shifts towards high temperatures the neutral desorption peak, meaning higher desorption energies. Ionic desorption spectra, such as those plotted in Fig. 3, reflect the dramatic increase of the ion desorption energy with the cesium coverage, due to the extra electric field produced by the adsorbed ions.

The electrostatic energy analyzer commonly used in AES can also be used in electron loss spectroscopy when looking at the energy losses of the elastically reflected primary electrons. Some energy loss spectra are shown in Fig. 4. First plasmon losses (around 2 eV) are observed above the cesium coverage which can be associated with the transition from the predominantly adsorbed ionic state to the neutral state. The A-B-C have been identified with ionization losses from O_2, O_3, and O_1 energy levels of adsorbed cesium. Ignoring possible change in relaxation effects after the ionization, then the shifts in energy when the

cesium coverage is increased (see Fig. 4) reflect the shifts in the binding energies of these respective levels when the state of cesium adsorption changes from the ionic to the neutral state.

The extra features A'-B'-C' have been, more tentatively associated with additional plasmon losses of the electrons that have suffered ionization losses or with interfacial excitations.

Particular emphasis will now be placed on the cesium-oxygen coadsorption in the continuation of this work.

References:

1. J. L. Desplat and J. L. Denisot; Thermionic Conversion Specialist Meeting, Eindhoven (Netherlands), Sept. 1975.
2. H. Niehus and E. Bauer; Surface Science, 46, 22, 1975.
3. A. G. Fedorus and A. G. Naumovets; Surface Science, 21, 426, 1970.

(J. L. Desplat)

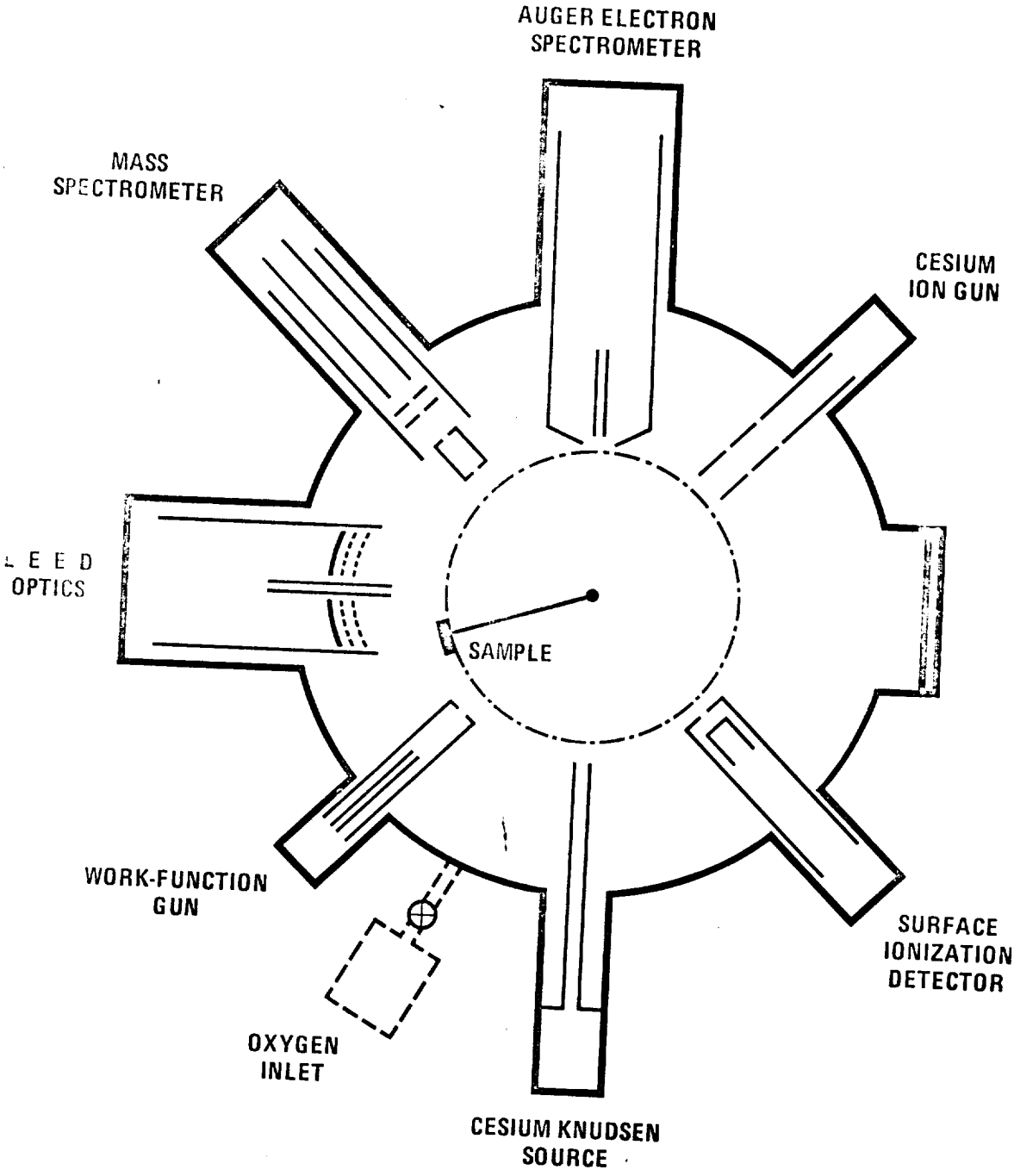
AUGER ELECTRON
SPECTROMETER
MASS
SPECTROMETER
CESIUM
ION GUN
L E E D
OPTICS
SAMPLE
WORK-FUNCTION
GUN
SURFACE
IONIZATION
DETECTOR
OXYGEN
INLET
CESIUM KNUDSEN
SOURCE

FIG.1

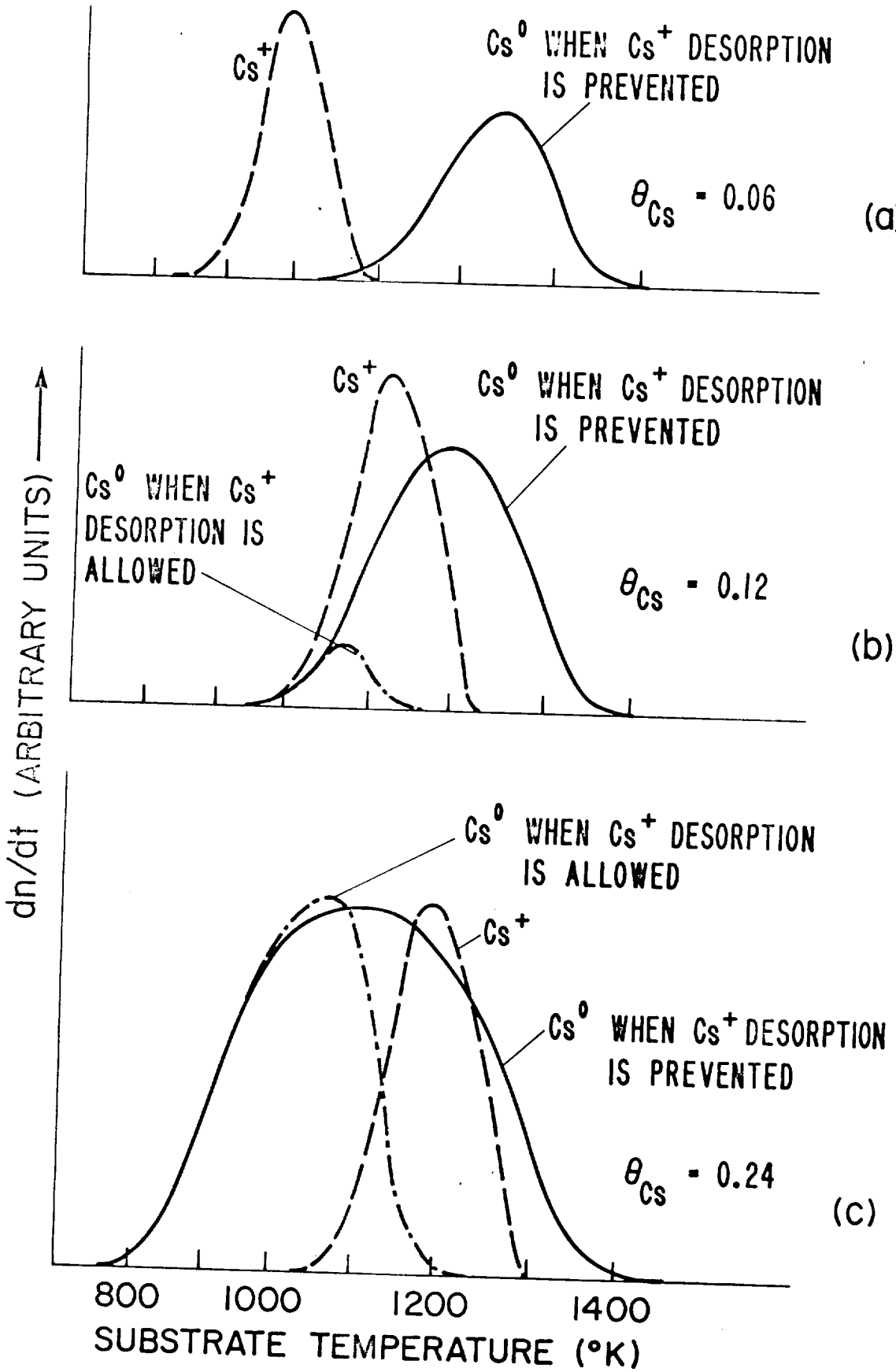
Cs+
Cs0 WHEN Cs+ DESORPTION IS PREVENTED
θCs = 0.06
(a)
Cs+
Cs0 WHEN Cs+ DESORPTION IS PREVENTED
Cs0 WHEN Cs+ DESORPTION IS ALLOWED
θCs = 0.12
(b)
dn/dt (ARBITRARY UNITS)
Cs0 WHEN Cs+ DESORPTION IS ALLOWED
Cs+
Cs0 WHEN Cs+ DESORPTION IS PREVENTED
θCs = 0.24
(c)
800
1000
1200
1400
SUBSTRATE TEMPERATURE (°K)

FIG. 2

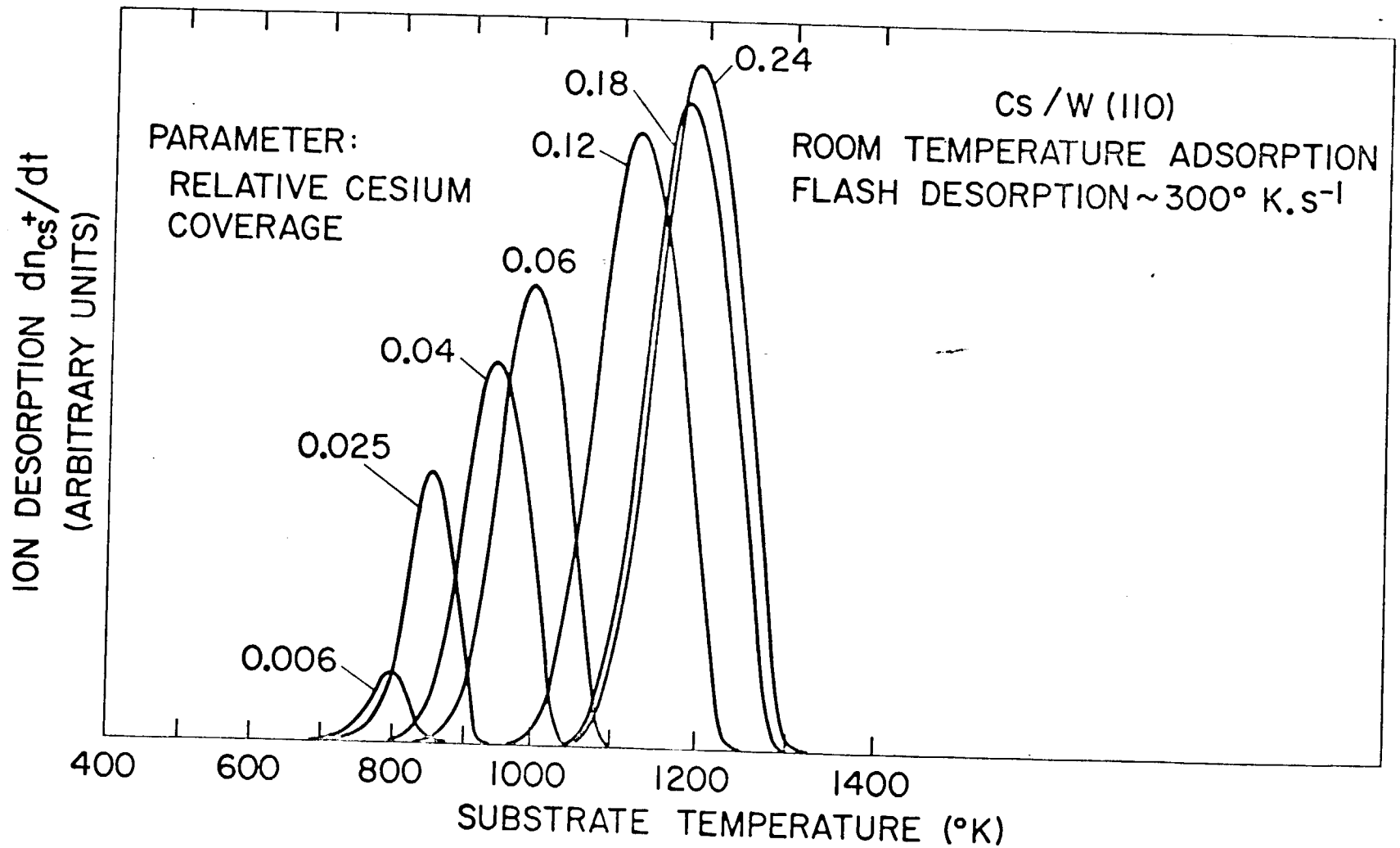
ION DESORPTION dn_{Cs^+}/dt
(ARBITRARY UNITS)
PARAMETER:
RELATIVE CESIUM
COVERAGE
0.006
0.025
0.04
0.06
0.12
0.18
0.24
Cs / W (110)
ROOM TEMPERATURE ADSORPTION
FLASH DESORPTION ~ 300° K. s^{-1}
400
600
800
1000
1200
1400
SUBSTRATE TEMPERATURE (°K)

FIG. 3

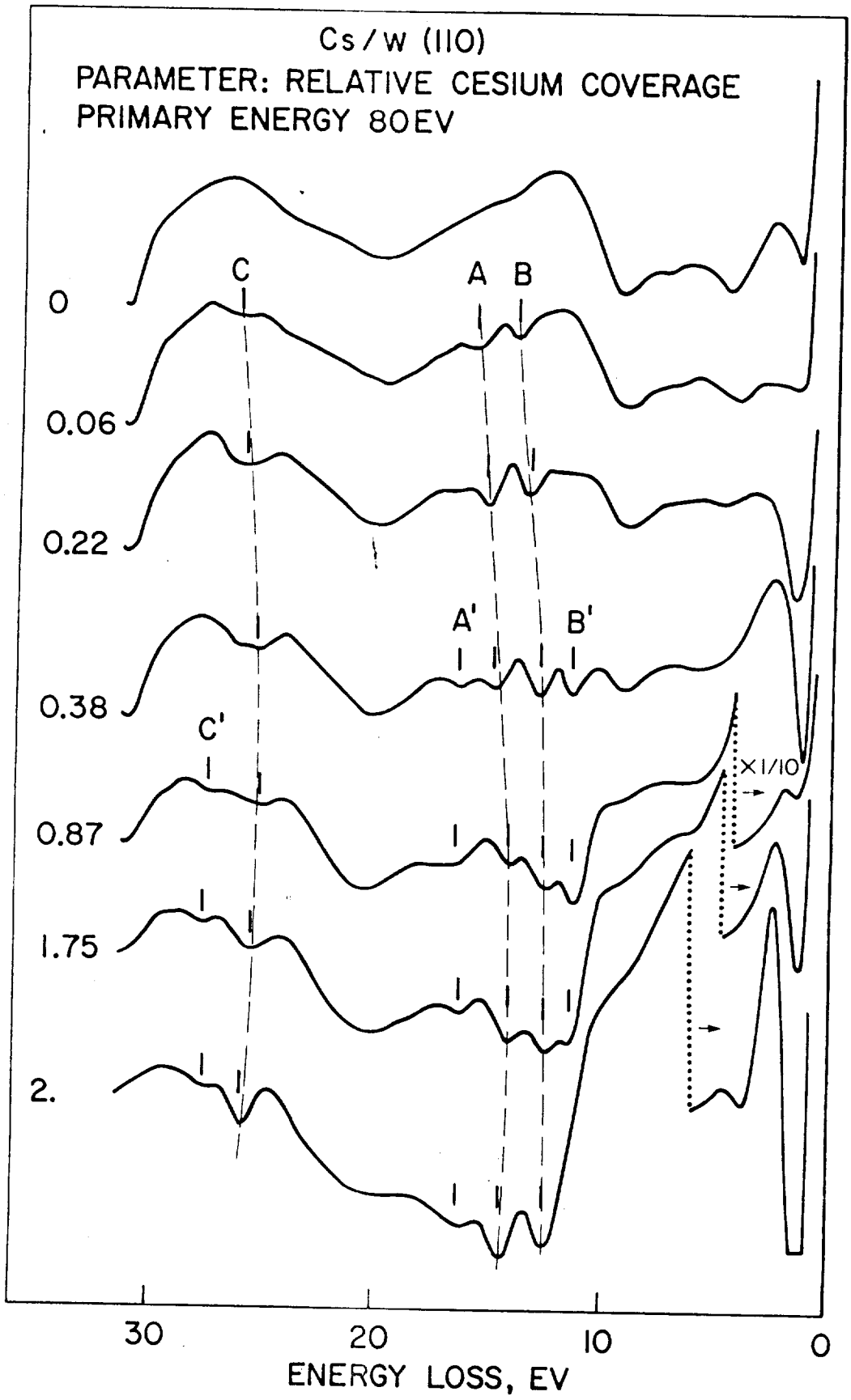
Cs / W (110)
PARAMETER: RELATIVE CESIUM COVERAGE
PRIMARY ENERGY 80EV
0
0.06
0.22
0.38
0.87
1.75
2.
C
A
B
A'
B'
C'
X1/10
30
20
10
0
ENERGY LOSS, EV

FIG. 4

PRESENT STATUS OF THE AUGER-MICROPROBE DEVELOPMENT. The most promising technique for high spatial resolution elemental analysis is Auger electron spectroscopy, which may approach the scale of resolution of the scanning electron microscope for topographical detail since both the Auger electrons (elemental information) and the secondary electrons (topographical information) are of the same magnitude in energy. In order to perform Auger electron spectroscopy in conjunction with scanning electron microscopy, the electron-optical column of a field emission SEM has been adapted to a UHV research chamber which incorporates a specimen manipulation system allowing high specimen stability, ion bombardment specimen cleaning, and multiple specimen handling under UHV. A discrete point line analysis monitoring the 1396 eV Al Auger peak across the boundary between the SiO_2 substrate and an Al pad of an MOS device indicates an edge resolution at least as good as 5000 Å.

(G. Todd)

CO-ADSORPTION OF Cu AND O ON (100)W. The co-adsorption of Cu and O on a (100)W surface was studied at temperatures between 300K and 1000K under ultrahigh vacuum conditions. This work is a natural extension of previous experiments on the Cu/(100)W[1] and O/(100)W[2] systems. The same experimental techniques used in the previous experiments, i.e., Auger electron spectroscopy (AES), low energy electron diffraction (LEED), work function change measurements ($\Delta\phi$) and thermal desorption spectroscopy (TDS), have been used in the present study. Adsorption was performed sequentially, with either Cu or O as the first adsorbate.

For pre-adsorption with O, at either 300K or 1000K, it was found that subsequent Cu adsorption at 300K is essentially independent of O coverage. Copper adsorption at 800K, however, depends on O coverage in the following way: The total amount of Cu on the surface, as measured by TDS, is essentially independent of O pre-adsorption, but the AES Cu peak amplitude (58/61 eV peak) depends on O coverage. The meaning of this result is that 2-dimensional Cu and O adsorption is additive, and that 3-dimensional condensation of Cu into small clusters occurs when the first adsorption layer is filled. Because of the small surface area of condensed Cu clusters, a sharp break in the Auger amplitude vs. deposition time curve results. A plot of the Cu Auger amplitude at which the break occurs, as a

function of coverage pre-adsorbed O, gives a nearly linear relationship, which can be expressed as $\Theta_{Cu} = 2\ (1 - \frac{4}{5}\ \Theta_O)$, where Θ_{Cu} and Θ_O are the fractional monolayer coverages of Cu and O, respectively. When Cu is adsorbed at temperatures above 950K onto a surface preadsorbed with O, the actual amount of Cu which sticks (as measured by subsequent TDS) decreases with increasing Cu and O coverage, i.e., the Cu sticking coefficient is no longer unity.

Different results are obtained for Cu preadsorption followed by O adsorption. Low temperature adsorption of O depends slightly on the structure of the preadsorbed Cu layer. The net effect, however, is that for Cu preadsorbed at 300K or 800K, the sticking probability of O is somewhat decreased from that on the clean W surface. Oxygen adsorption at 800K or 1000K yields more striking results. The Cu Auger signal shows an initial gradual decrease, followed by a rapid decrease during continued O adsorption. TDS data show that the gradual decrease is not accompanied by any desorption of Cu, nor is the decrease to be explained by agglomeration of Cu into clusters. The rapid Cu AA decrease is, however, attributable to clustering and partially to desorption (T=1000K). In contrast to the case of 800K Cu adsorption on a preadsorbed O layer, it should be noted that in this case O is replacing Cu already tightly adsorbed on the W surface. At the high temperatures used, Cu can be desorbed even though it would be stable as an adsorbed monolayer on W, because the Cu-Cu binding energy is somewhat less than the Cu-W binding energy[1]. Therefore, the total amount of Cu present, as observed by TDA, decreases with increasing time at 1000K, after agglomeration has occurred. Another remarkable effect can be seen from Fig. 5: The saturation coverage of O increases with increasing amount of preadsorbed Cu. This result is interpreted by roughening of the (100)W surface caused by the preadsorbed Cu at high temperature, thereby creating more adsorption sites for O [1]. In support of this interpretation, LEED experiments have shown microfacetting of the surface to occur.

References:

1. E. Bauer, H. Poppa, G. Todd and F. Bonczek: J. Appl. Phys. 45 (1974), 5175.

2. E. Bauer, H. Poppa and Y. Viswanath: Surface Science 59 (1976), in press.

(E. Bauer, H. Poppa, Y. Viswanath and P. R. Davis)

OXIDE FORMATION ON SINGLE CRYSTALLINE COPPER-NICKEL ALLOY THIN FILMS. Single crystalline 600-1000 A thin films Cu-3-5% Ni and Cu-50% Ni alloy were prepared by vapor deposition onto (001) NaCl substrates and oxidized in-situ at 425°C and 5×10^{-1} Pa oxygen partial pressure under controlled residual gas environment conditions in a high-resolution transmission electron microscope. For both ranges of alloy concentration, Cu_2O and NiO were observed to grow independently. No mixed oxides were observed.

The low-concentration nickel alloys exhibited a reduced induction period for Cu_2O when compared to pure copper films. In the initial phase of Cu_2O precipitation, contrast features were observed that can be explained as due to strain fields induced by the Cu_2O crystallites in the matrix. This indicates a two-dimensional nucleation behavior of Cu_2O. The oxidation rate normal to the film surface was then observed to be fast, resulting in a through-depth oxidation of the alloy film shortly after first appearance of oxide on the film surface. The lateral growth behavior of CuO crystallites was very similar to that found in previous work on pure copper films, i.e., the nickel in the matrix did not significantly influence the copper oxidation products. On the other hand, the nickel oxidation products (NiO) did exhibit significant differences in number density, shape, and growth rate when compared to oxidation of pure nickel films. They did, however, grow on top of the alloy film, which is in agreement with the mentioned pure nickel-oxidation experiments. These findings were explained by a previously established Cu-Cu_2O oxidation mechanism involving growth which is based on surface diffusion of oxygen and in-place oxidation of copper at the Cu_2O metal interface, in conjunction with a simultaneous NiO oxidation mechanism which is based on Ni diffusion in the matrix to the sites of NiO growth.

The basic finding for the oxidation of Cu-50% Ni alloy films was that in this case both Cu_2O and NiO grew in virtually exactly the respective pure metal oxidation modes, which can again be explained by the above growth mechanisms. It was found and can be understood for the cation-diffusion controlled NiO growth that the induction period for NiO formation was extremely low and that the induction period for Cu_2O precipitation was prolonged due to the rapid initial oxygen uptake in the nickel oxidation process.

The work reported here fills part of a gap in the understanding of the oxide nucleation and initial growth process

of substitutional alloys with multiple oxides and indicates that the predominant factors that determine the initial oxidation behavior are the diffusivities of the involved species.

(K. Heinemann)

CORROSION OF STRUCTURAL ENGINEERING MATERIALS IN COAL GASIFICATION ENVIRONMENTS. Sulfidation of SAE 310 stainless steel has been completed as a function of sulfur potential and temperature. At a fixed temperature of 1065°K, the sulfidation kinetics, composition and morphology of sulfide scale formation were studied over a range of sulfur potentials from $1.5 \times 10^{-4} Nm^{-2}$ to $9 \times 10^{2} Nm^{-2}$. At all sulfur potentials investigated, the sulfide scales were bound to be multilayered. The outer layer consists of Fe-Ni-S, the middle layer consists of a mixed thiospinel of variable composition $Fe(Fe_{2-x}Cr_xS_4)$ and the inner layer consists of dispersed sulfides (rich in chromium) in a metal matrix (nickel and iron). The relative thickness of the individual layers as well as composition were found to depend on the sulfur potential. The outer layer thickness progressively decreased as the sulfur potential decreased whereas the middle layer thickness increased and the inner layer thickness remained essentially constant. At very low sulfur potentials the outer layer disappeared completely. Finally, at higher temperatures (T>1145°K) where the conditions are favorable for the formation of an outer layer, the outer layer became a liquid and the melt separated into a two phase solid upon cooling, viz: sulfide phase containing iron-nickel sulfide and metallic phase containing iron and nickel. At all sulfur potentials investigated, the reaction rate was found to obey a parabolic rate law after an initial transient period. Extended transient periods could be attributed to unsteady state conditions resulting from compositional variations in the middle layer. The growth of the outer layers was found to be primarily due to the transport of cations whereas the inner layer growth was due to the dissociation of the primary product at the alloy scale interface and depended on the availability of chromium. The overall rate controlling step was found to be the diffusion of metal ions through the middle layer.

(D. B. Rao and H. G. Nelson)

THE KINETICS OF HYDROGEN CHEMISORPTION ONTO EVAPORATED IRON FILMS. Since our previous work had shown that under certain conditions the reaction step connecting the precursor state with the chemisorbed state can be the rate limiting step for adsorption, measurements have been undertaken to determine the activation energy for this step. Our best estimates to date are for an activation barrier of approximately .25eV/molecule, which is in reasonable agreement with other related work. The value of the absolute rate constant which connects the chemisorbed state with the precursor state has also been indirectly determined. The temperature dependence of this rate is in disagreement with intuitive expectation suggesting that either; (1) additional new physics is entering into the phenomena, or (2) there is a breakdown in the basic kinetic model which is being used to describe the chemisorption process. The resolution of this problem is being explored both theoretically and experimentally by improving the accuracy of the measurements to allow for a more careful comparison of the kinetic model with the data.

(M. R. Shanabarger)

THE KINETICS OF THE INCUBATION PERIOD OF HYDROGEN ATTACK IN LOW CARBON STEELS. A program has been recently undertaken to characterize and understand the kinetics of the initial processes which occur during the incubation period of hydrogen attack (HA) of steels. The two dominant processes involved are believed to be; (1) internal decarburization, and (2) fissure growth. Internal decarburization is a process during which, at elevated temperatures and pressures, carbon in the steel reacts with dissolved hydrogen at high energy sites, such as grain boundaries or at inclusions, to form methane. Methane formed under these conditions cannot diffuse through the lattice to the surface of the steel and escape into the atmosphere. Instead, the trapped methane gas builds up a pressure and eventually causes nucleation and growth of fissures within the steel. The immediate task of acquiring equipment and setting up an apparatus for monitoring changes in the dissolved carbon concentration has been undertaken. The dissolved carbon concentration will be monitored via changes in the electrical resistance of the steel. A wheatstone bridge circuit has been designed for use with wire samples. The measurements will take place inside a chamber which can be pressurized (100-1500 psi) at elevated temperatures (300-700°C). This arrangement will

permit monitoring the resistivity changes continuously. At present important measurement parameters such as sensitivity and error sources are being evaluated.

(K. Shah and M. R. Shanabarger)

STRESS CORROSION OF ZIRCALOY. The stress corrosion cracking of annealed Zircaloy-4 exposed to high purity iodine at 633°K was studied in an effort to establish the threshold stress intensity (K_{Iscc}), the crack velocity at low values of stress intensity, the effect of free iron on the values of K_{Iscc} and crack velocity. Compact tension-type WOL specimens were prefatigue cracked in air, wedge-opened using a Molybdenum alloy, encapsulated in a glass tube with 4.4 mg of iodine per cm^2 of zircaloy, sealed and placed in a furnace at 633°K for various lengths of time. Specimens with a stress intensity of $\sim$6-7 $MPam^{\frac{1}{2}}$ failed to undergo any observable stress corrosion cracking. However, specimens loaded to higher initial stress intensities did exhibit some subcritical crack growth. A crack propagation rate of $\sim 7 \times 10^{-9} ms^{-1}$ and a K_{Iscc} of $\sim$10MPam were calculated from the final fracture parameters. The specimen which contained only the machined notch failed to undergo any observable stress corrosion cracking. This result indicates that the crack initiation process may be important; however, further tests to assess the roles of such factors as surface oxide and plastic zone must be performed. Iron wool in the capsule slowed the crack growth rate by $\sim$50%, but did not appear to change the K_{Iscc}. Fractographic analysis of the stress corrosion areas indicated that crack growth occurs by transgranular cleavage and a mode similar to that observed in the aqueous chloride stress corrosion cracking of titanium alloys.

(H. Wachob and H. G. Nelson)

HYDROGEN-ENHANCED CRACK GROWTH IN A LOW STRENGTH FERRITIC STEEL. Hydrogen-induced slow crack growth of a low strength, low carbon, ferritic steel has been investigated under conditions of static and cyclic loading in a vacuum, a high purity hydrogen, and a hydrogen sulfide environment at room temperature. Although no evidence of slow crack growth was observed under conditions of static loading in these environments, under conditions of cyclic loading Stage II fatigue crack growth was found to be significantly enhanced by the presence of both a hydrogen and a hydrogen

sulfide environment compared with a vacuum environment. The primary influence of hydrogen was to increase crack growth rate while retaining the functional dependence, $da/dN \alpha \Delta K^{3 \cdot 6}$, observed in vacuum. At a cyclic frequency of 1 H_2 hydrogen-enhanced crack growth was found to be a maximum (da/dN being $\sim$100 times faster than in vacuum) at a hydrogen pressure of $\sim$2000 kN m^{-2} and at a hydrogen sulfide pressure of 1 kNm^{-2} with no further enhancement observed at higher pressures. Additionally, hydrogen-enhanced crack growth was found to be independent of: R ratio (k_{min}/k_{max}) at R ratios between 0.15 and 0.37; of yield strength at yield strengths between 262 and 524 MNm^{-2}; of test frequency between 1 and 10 H_2 at hydrogen pressures equal to and greater than those at which maximum da/dN was observed; and, of form of loading (sine, square or saw-tooth wave). A mechanism has been developed to explain these observations and is based on increased ease of cross-slip due to hydrogen-dislocation interactions, a broadening of the slip band at the crack tip, and a resultant increase in crack growth rate under conditions of cyclic loading.

(H. G. Nelson)

THE KINETICS OF OXYGEN (O) AND HYDROGEN SULFIDE (H_2S) CHEMISORPTION ONTO EVAPORATED IRON (Fe) FILMS. Utilizing the techniques of chemisorption induced change in the electrical resistance of polycrystalline Fe films combined with Auger Electron Spectroscopy of the oxygen Auger transition, a study has been completed of the room temperature adsorption kinetics of the O/Fe system and preliminary corresponding measurements have been made for the H_2S/Fe system. The correlated measurement techniques show that molecular oxygen adsorbs dissociatively onto Fe via a single adsorption step with a coverage independent sticking coefficient of .02. This strongly suggests that the adsorption process is thermally activated. These measurements have established the origin of the resistance change as arising from the localization of conduction electrons (initially non-localized) to localized sites at the surface which are directly associated with the oxygen adatom. The measurements indicate that approximately two conductron electrons are localized per oxygen adatom. Preliminary measurements on H_2S adsorption have shown that this molecule adsorbs via a first order process. The unusual behavior of the initial resistance change may permit future work to identify the mechanisms and steps

associated with the dissociation of the H_2S molecule on Fe. Co-adsorption of H_2S and O_2 have demonstrated that the oxygen always penetrates under the sulfur overlayer, irrespective of which overlayer formed first. Additional analysis of the co-adsorption experiments suggests that the sulfur and oxygen are adsorbed in different Fe sites and that when both overlayers are present they form an SO_2 complex with the oxygen binding the SO_2 complex to the Fe. In addition at room temperature, the formation of an oxide layer is not observed for oxygen exposures <3000 μtom. sec. which is in contrast to other work.

(M. R. Shanabarger and R. D. Moorhead)

THE SURFACE MOBILITY OF SMALL METAL CLUSTERS. The mobility behavior of small clusters on solid surfaces is of importance to the understanding of some basic phenomena in catalysis. Mobility leading to coalescence changes the surface to volume ratio of the catalysts and therefore also the catalytic activity. Repulsive forces between catalytic particles on the other hand could reduce agglomeration leading to a maximizing of cluster nearest neighbor distances which would improve the stability of the catalytic properties of a system.

Basic in-situ experiments were conducted under controlled conditions to gain information about the low temperature cluster mobility mechanism and in particles about the coalescence and the Ostwald ripening mechanisms of metal atom clusters. The following systems were examined: Silver on amorphized graphite, gold on (001) MgO, and gold on (111) MgO.

In the case of Ag/C, the support films were prepared by the gelatine-cleavage method and cleaned inside the UHV specimen chamber of the in-situ high-resolution, transmission electron microscope used for the experimentation by argon ion beam sputtering. Small amounts of silver (approx. 1 A average thickness) were deposited by electron beam evaporation. The particle number density and mean diameter were 4×10^{12} μm and 14 A, respectively. The following main observations were made for Ag/amorphized graphite: (1) Ostwald ripening was observed. It would take as much as one hour for one 12 A-particle to disappear by atom-to-atom surface diffusion to large neighboring clusters; (2) Several

different types of cluster mobility events were observed, all leading to coalescence. A clear distinction between the cluster mobility phase and the sintering phase of coalescence was found.

Thin, transparent areas of MgO were prepared in-situ by electron-beam cleavage immediately prior to the gold deposition. The experiments on (001) MgO surfaces yielded a mobility behavior leading to coalescence only in 20% of all observed mobility events. In 80% of the cases, the particle movements occurred into open spaces between neighboring particles. Curved trajectories were measured indicating repulsive forces that tend to maximize the nearest neighbor distances. Such repulsive forces have been previously postulated as due to overlapping strain field induced by the gold clusters in the substrate and were experimentally demonstrated by post-test measurements of the radial distribution functions of the deposit atom clusters. The present results, are a direct proof of repulsive forces and include kinetic measurements. The cluster speeds during mobility are of the order of 500-1000A/sec, and the movements occur frequently in an oscillatory fashion.

For (111) MgO, distinct rotational alignments of clusters on the substrate were found. The final azimuthal orientation of rotating particles was epitaxial, and it was concluded that non-epitaxy may be a necessary condition for particle mobility at low temperatures.

(K. Heinemann, J. J. Metois and H. Poppa)

THE ADSORPTION AND EARLY STAGES OF CONDENSATION OF Ag AND Au ON W SINGLE CRYSTAL SURFACES. Ag and Au are evaporated to coverages up to several monolayers and in the temperature range between 300K and 1300K, onto W(110) and (100) single crystal surfaces. The mode of growth, the structure of the layers and the crystallographic anisotropy of adsorption and condensation are studied by Auger electron spectroscopy (AES) and low energy electron diffraction (LEED). The results are compared with thermal desorption spectroscopy (TDS) data. Absolute deposition rates (±10%) have been monitored with a quartz oscillator. For clarity, a description of the methods used is given for the particular case of Au/(110)W only, and then general conclusions are drawn.

The Au Auger amplitude (AA) increases with deposition time for two deposition temperatures. The deposition rates and Auger sensitivities differ slightly in the two experiments but in both three breaks are seen; corresponding to three layers of deposited Au. As judged by the relative deposition times and AA's, the amount of Au incorporated into the first layer at 300K is only about 90% of that incorporated at 1050K. This is not surprising because many atoms have to be displaced in order to accommodate the last 10% of the atoms which requires thermal activation. The absolute saturation coverages of the various layers as indicated by the linear segments and the breaks in the AA vs. t curves are: 28×10^{14} atoms cm^{-2} for the second break as determined by the quartz oscillator, 13×10^{14} atoms cm^{-2}, 29×10^{14} atoms cm^{-2} and 44×10^{14} atoms cm^{-2} for the first, second and third layer breaks, respectively, as determined by LEED (see below) for the 1050K layers. After completion of the third monolayer, the AA increases only slowly with deposition time at 300K, is constant at 850K and even decreases at 1050K. Nevertheless, all Au condenses at these temperatures as the integrated desorption flux proves. The constant AA signal beyond $\theta = 3$ is therefore attributed to the formation of three-dimensional crystals contributing little to the Auger signal, the decrease to the incorporation of the Au atoms of the third layer into the three dimensional crystals which are formed beyond $\theta = 3$. This behavior is similar to the instability of the third layer of Cu on W(110).[1]

The influence of temperature on adsorption and desorption shows a decrease of the AA and of the integrated desorption flux with increasing deposition temperature for an exposure of 3/4 m.l. It is apparent that condensation is complete up to 1150K, but that the sticking coefficient decreases rapidly above 1200K.

General Conclusions

1. An adsorption layer consisting of 2-3 monolayers, depending on the surface orientation of W, is formed before three-dimensional crystallization begins. At low temperatures - which in the case of Au may be as high as 800K - one or more additional monolayers may form which are metastable, however, and which coalesce into three-dimensional crystals upon heating.

2. The structure of the layers changes with coverage and temperature. On the less dense packed W(100) surface the structure is much more influenced by the substrate than on the close packed (110) surface, on which essentially only the first layer is strongly deformed by the influence of the substrate surface potential. On the (100) surface the substrate determines the structure of the entire adsorption layer in the case of Ag, but in the case of Au only the structure of the first two monolayers is determined by the substrate. Two temperature regimes can be distinguished on the W(100) surface in which the structures differ, the system Au/W being distinguished by a particularly large variety of structures.

3. For the vapor fluxes used (some 10^{12} atoms cm^{-2}) the sticking coefficient remains constant up to relatively high temperatures. These critical temperatures are about 900K and 1100K for Ag and Au, respectively, on the {100} surface. The temperature at which the sticking coefficient decreases depends on surface orientation and on coverage. This is also the case for the temperatures at which the layers start to desorb.

4. The fcc/bcc interfacial orientation relationship is different for Ag and Au. On the {110} surface the Ag/W interface has the Kurdjumov-Sachs orientation relationship, i.e., $(111)_{fcc}$ $(110)_{bcc}$, $[110]_{fcc}$ $[111]_{bcc}$ which is equivalent to $[1\bar{1}2]_{fcc}$ $[1\bar{1}2]_{bcc}$. The Au[110] axis is rotated 2.3° from the [001] axis of W towards the Kurdjumov-Sachs relationship which is obtained by a rotation of 5 1/4°. There is no indication of the existence of an interfacial layer with a periodicity different from the bulk. Only in the case of Au is a minor lattice contraction observed. This contraction may, however, be present only in ultrathin films but not at a bulk interface. On the {100} surface the interfacial orientation relationship could be established only for Au: $(111)_{fcc}$ $(100)_{bcc}$, $[110]_{fcc}$ $[001]_{bcc}$. In this case, also, a compression was observed for Au which may not be present in a bulk interface. Futhermore, a pseudomorphic Au monolayer is sandwiched between the compressed Au layer and the W surface.

(E. Bauer, H. Poppa, G. Todd and P. Davis)

Technology Development Branch

1. Thermal Control - Heat Pipe Technology

THERMAL CONTROL - HEAT PIPE TECHNOLOGY. The objectives of the Ames heat pipe program are: (1) To establish flight-level confidence in advanced heat pipe technology through flight tests; (2) to develop basic control mechanisms, allowing variable-conductance, feedback-control, and diode operation; and (3) to develop improved liquid transport capacity and reliability. Continuing progress in all of these areas is being made.

The Ames Heat Pipe Experiment aboard the Orbiting Astronomical Observatory (OAO-3) showed excellent performance throughout 4-1/2 years in orbit. The Advanced Thermal Control Flight Experiment on ATS-6 continues to operate well after 2-1/2 years. Ames and Goddard are cooperating on a Heat Pipe Package (HEPP) for the March 1978 Tiros-N launch. Ames is providing a blocking orifice cryogenic diode heat pipe capable of cooling and protecting equipment such as infrared detectors.

In-house investigations of basic control mechanisms include tests and analysis of gas-controlled, grooved, cryogenic variable conductance pipe which have shown encouraging results.

Other programs are improving base heat pipe technology. A program to develop hydrogen heat pipes for isothermalization of cooled optics and other applications has just been initiated. Two flexible cryogenic heat pipes representative of radiator deployment or movable detector applications have been fabricated and are under test. Pipes with axially-varied porosity have tested successfully with fluids which cover the 100-200K range.

Two promising techniques to improve heat pipe capacity, the "inverted meniscus" evaporative surface and the jet-pump assisted artery, have successfully completed proof-of-principle experiments. Heat pipes incorporating these features are being designed, built, and tested.

Communication with Air Force heat pipe users has been maintained in accord with the OAST/AFSC interdependency agreement. Where appropriate, Air Force requirements have been factored into the OAST program.

The thrust of the Ames program continues in the direction of cryogenic temperatures where many potential applications exist and where advances promise to allow substantial improvements in instrument sensitivity and stability.

(C. R. McCreight)

HEAT PIPE PACKAGE (HEPP) FOR TIROS-N

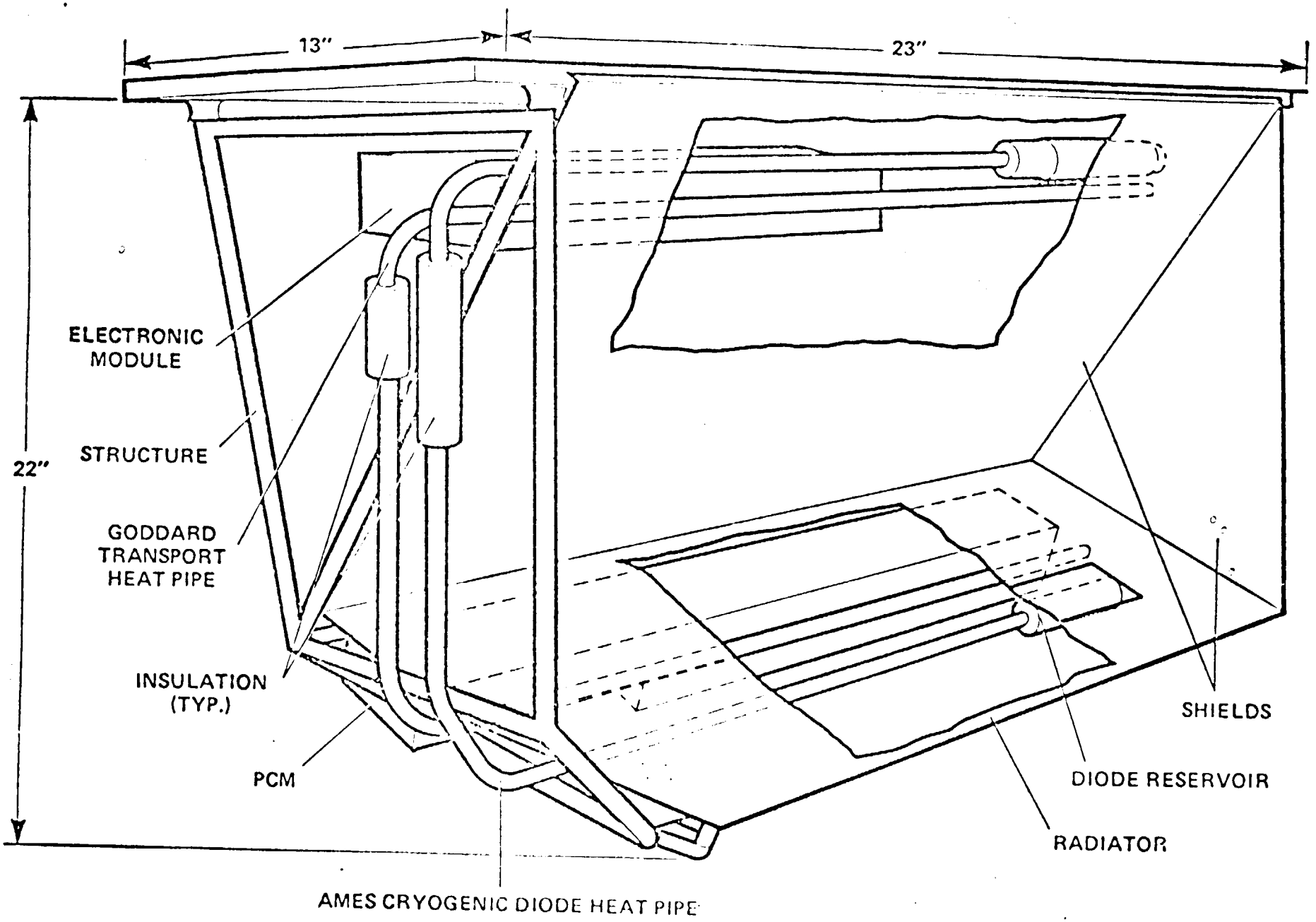

Entry Technology Branch

1. Advanced Thermal Protection Materials
2. Hyperpure Silica Heat Shields

ADVANCED THERMAL PROTECTION MATERIALS. Ames Research Center is developing improved reusable heat shield materials for advanced Space Shuttle, Earth Orbital Transportation Systems and other related applications.

The Ames developed Reaction Cured Glass (RCG) coating was adopted in May by the Space Shuttle program for coating the orbitor silica RSI heat shield. Extensive testing by LMSC, JSC and Ames showed the RCG coating to be far superior to the then baseline system.

Martin Marietta Corporation has demonstrated their capability to manufacture Ames silica RSI and is now making it in small quantities for evaluation.

A new 6 lb/ft^3 silica RSI has been developed and is currently being evaluated. It has properties equivalent to the current 9 lb/ft^3 material except that its distortion temperature is about 100°F lower.

A new series of reaction cured glass coatings has been developed which offer improved optical properties, lower glazing temperature and other improvements over the current coating. They are now being evaluated.

(H. Goldstein)

HYPERPURE SILICA HEAT SHIELD. A hyperpure vitreous silica material is being developed for use as a reflective and ablative heat shield for planetary entry. Various purity grades and forms of raw materials were evaluated along with various processing methods. All are critically important to the success of this concept. Slip casting of high purity grain was selected as the best processing method, resulting in a highly reflective material in the wavelength bands of interest (the visible and ultraviolet regions).

The selected material was characterized with respect to optical, mechanical and physical properties using a limited number of specimens. The process has been scaled up to produce a one-half scale heat shield (18 in. dia.) for a Jupiter entry vehicle.

This work is now being extended to improve the structural safety factor of the heat shield by making the hyperpure silica material tougher through the addition of silica fibers. This work is being done by McDonnell Douglas Astronautics Company-East under NASA Contract NAS2-7897.

(P. Nachtsheim)

PRELIMINARY COMPARISON OF TOUGHER FUSED SILICA MATERIALS